PHY 122B Muon Lifetime Lab report

Guanyu Qian
University of California, Davis

June 3rd 2022

Abstract

The objective of this experiment is to examine the muon mean lifetime using a system containing a plastic scintillator, a photomultiplier tube, and a logic circuit. The motivation of the experiment is that, as one of the elementary particles, determining muon lifetime can build a foundation for exploring advanced particle physics. The overall methodology used is to use a plastic scintillator as the stopping medium for muons. As muons stop and decay in the medium, light pulses are sent from the scintillator to the photomultiplier tube. Consequently, it outputs a negative pulse to the logic circuit that discriminates the pluses, converts the timing sequence into voltage, and feed data into the data acquisition system. The experiment is conducted three times with two 120-hours runs and one 40-hour run. A exponential lift, $N(t) = N_0 \cdot e^{-\frac{t}{\tau}} + B$, is applied to the re-binned data. The measurement result of muon lifetime, τ_{mu}, is 2.319 μs $\pm$ 0.062 μs (stat) $\pm$ 0.031 μs (syst), 5% different from the publish value, 2.196 μs.

1 Introduction

The muon was an elementary particle first discovered in 1936. It is now also known as one of the six leptons. Although muons have the same properties as electrons, they have a much larger mass, around 207 times heavier than an electron. Thus, the enormous mass difference makes muons unstable and undergoes a decay process. This experiment aims to measure the muon mean lifetime primarily based on a plastic scintillator connected with a photomultiplier tube and a logic circuit.

1.1 Formation of Muons

Muons are produced in the high-energy collision process when a proton from the cosmic ray hits a molecule in the Earth's atmosphere. As shown in Fig 1, three types of pions, π^-, π^+, and π^0, are formed during the collision. Then, charged pions, π^- and π^+, decay into μ^- and μ^+ and muon neutrinos, described in Eqn 1. As a result, muons that travel from the atmosphere to the sea level are detected by the scintillator during the experiment.

$$\begin{aligned} \pi^+ &\longrightarrow \mu^+ + \nu_\mu \\ \pi^- &\longrightarrow \mu^- + \overline{\nu}_\mu \end{aligned} \tag{1}$$

However, the Earth's atmosphere is 12 km from the sea level, while muons only have a mean lifetime of a few microseconds. In other words, muons' lifetime does not last long enough for them to travel from the upper atmosphere to the sea level. Nevertheless, since muons move at a relatively high velocity, they experience a time dilation, as shown in Eqn 2. It implies that the time is slowed down in the muons' frame of reference, which becomes sufficient for muons to travel to the sea level.

$$\Delta t' = \frac{\Delta t}{\sqrt{1 - \frac{v^2}{c^2}}} \tag{2}$$

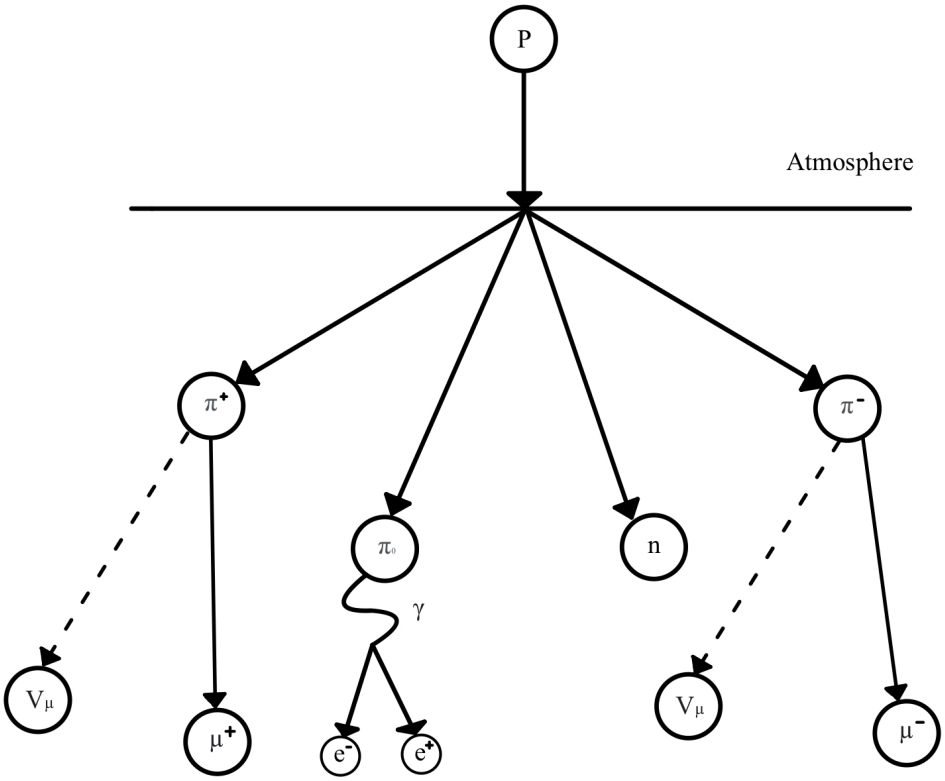

Figure 1: An illustration of the high-energy collision between the molecule and the cosmic ray. As the proton in the cosmic ray hit the air molecule in the atmosphere, three types of pions are produced, and charged pions will decay into μ^+ and μ^+. These muons can travel from the upper atmosphere to the sea level due to the time dilation.

1.2 Detecting Muons

The detecting mechanism of stopped and decayed muons is to use a scintillating medium that absorbs the energy of muons when they enter the medium. In this way, the energy of muons that pass through the medium would cause de-excitation of the atoms and generate light. For muons that stop in the medium, they would experience a decay process, which generates an electron, excites the scintillating medium, and generates light. Therefore, a plastic scintillator enclosed by an aluminum cube is used to detect the muons, as shown in Fig 2. Furthermore, a photomultiplier tube is connected to this

scintillator, which detects these light signals and outputs a negative signal (see section 2.1).

Numerous muons could enter the scintillator during the 5-day run. The estimation of incoming muons' rate can be calculated by integrating Eqn 3, an empirical formula approximating the intensity of the muons at sea level with different zenith angles.

$$I(\phi) = I_v \cdot cos^2(\phi) \tag{3}$$

I_v is a constant value of $0.0083\,cm^{-2}\,str^{-1}$ derived by Rossi in 1940. Angle ϕ refers to the zenith angle, which is estimated as $\frac{\pi}{4}$, as shown in Fig 2. The cross-section area of the scintillator is $(25cm)^2$. As a result, the scintillator will detect six muons per second, predicted by Eqn 4.

$$\int I(\phi)\,dA\,d\Omega = (25cm)^2 \cdot 0.0083\,cm^{-2}\,str^{-1} \int_0^{\pi/4} \int_0^{2\pi} cos^2(\phi) \cdot sin(\phi)\,d\theta\,d\phi \approx 6/sec \tag{4}$$

Furthermore, the muons lose 2 Mev of their energy per centimeter squared per gram passing through the medium. Therefore, the scintillator can only make muons with energy lower than 50 Mev stop in the medium, which only takes up 0.3% (see reference [6]) of the total muons detected. Thus, the expected muon stopped per second is $6 \times 0.3\% = 0.02$.

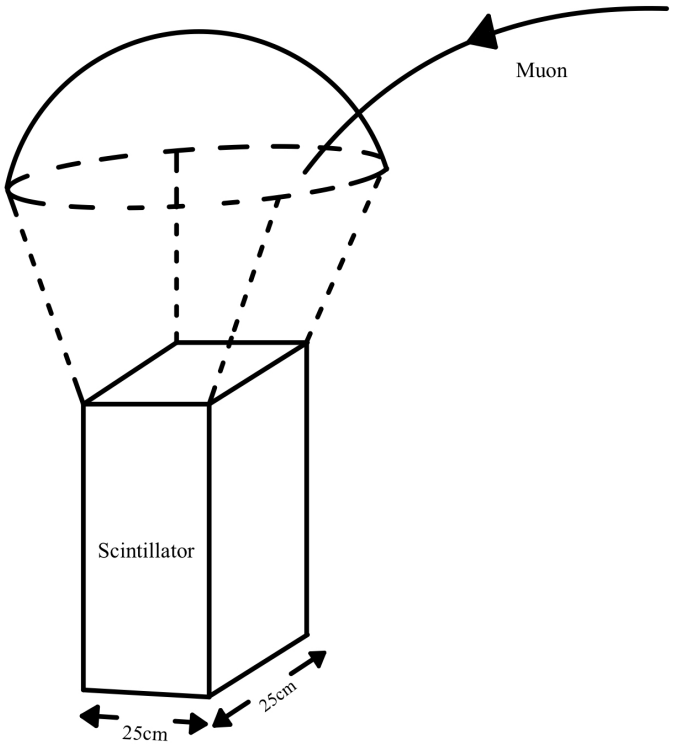

Figure 2: The mechanism of muons detection. The plastic scintillator is enclosed by an aluminum cube which has a cross-section area of $(25cm)^2$. However, muons cannot go through the scintillator from every direction. The estimated detectable azimuth angle is from 0 to 2π, and the detectable zenith angle is from 0 to $\pi/4$.

Consequently, two types of pulses and electronic noises will be detected, as shown in Fig 3. Two pulses are created from the muon stop and decay events. However, the

muon stop event is caused by the energy of a muon, while the decay event is caused by the energy of an electron emitted by the muon. By the conservation of energy, the pulse height of the muon decay event is smaller than the pulse height of the muon stop event. In this experiment, a threshold voltage was set to detect both pulses with different amplitudes while filtering out the noises from the electronics. (see section 2.2).

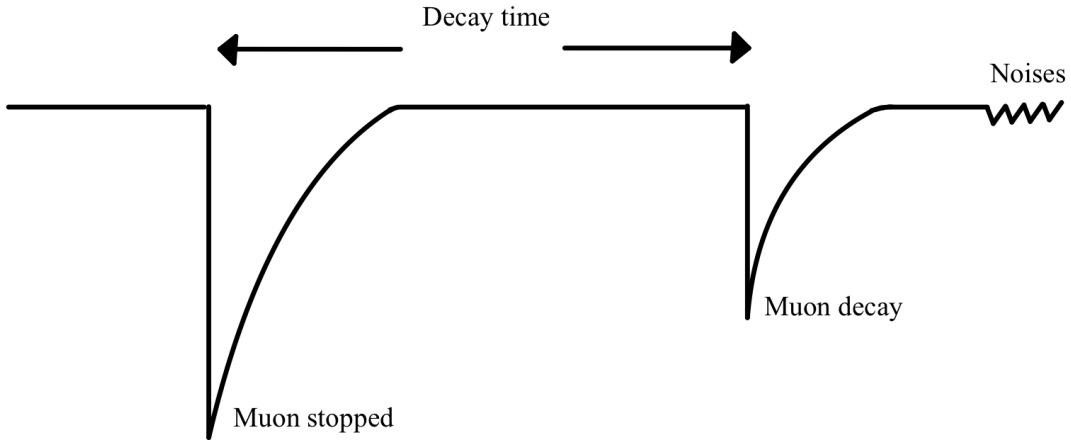

Figure 3: Theoretical waveforms of muon stop and decay pluses. Two types with different amplitudes are output by the photomultiplier tube. It is worth noting that electronic noises have a narrow gap between the muon decay pulse. Thus, a threshold level needs to be set to filter out these noises.

1.3 Decay Process

Muons share identical properties with electrons, except that muons are 207 times heavier. Due to this mass difference, muons will undergo decay and emit an electron, as shown in Fig 3. Furthermore, the positive and negative muon atoms decay process are described in Eqn 5. $\overline{v}_\mu$ and $\overline{v}_e$ are known as neutrinos, massless particles that Pauli first brought up to justify the conservation of energy in the decay process.

$$\begin{aligned} \mu^+ &\longrightarrow \mathrm{e}^+ + \mathrm{v_e} + \overline{\mathrm{v}}_\mu \\ \mu^- &\longrightarrow \mathrm{e}^- + \mathrm{v}_\mu + \overline{\mathrm{v}}_\mathrm{e} \end{aligned} \tag{5}$$

In this experiment, the focus is to measure the muon mean lifetime, τ. The calculation for muon mean lifetime is an analogy of Fermi's theory of the neutron's lifetime in 1932, as shown in Eqn 6.

$$\tau = \frac{\hbar}{\Gamma} = \frac{30\pi^3\hbar}{G^2E_0^5} \tag{6}$$

G is a constant value of $1.136 \times 10^{-5}\, GeV$ calculated by the half-life time of a neutron, and E_0 refers to the difference in nuclear energy, which equals 1.81 MeV. This equation can be used as an analogy to calculate the muon mean lifetime because both muons and neutrons are -1/2 spin particles. Therefore, Eqn 7 is used to derive the muon mean lifetime.

$$\tau = \frac{\hbar}{\Gamma} = \frac{192\pi^3\hbar}{G^2m_\mu^5} \tag{7}$$

The constant 30 is corrected to 192 due to the reason that the recoil of the final electron is not negligible in beta decay. Moreover, E_0 can be substituted by m_μ by making analogy. As a result, the accepted muon mean lifetime is 2.2 μs

However, in the experiment, the scintillator is incapable of distinguishing between μ^+ and μ^-. As a result, a capture effect can occur between μ^- and the carbon nucleus. This phenomenon has an impact on the muon lifetime calculation, which will be discussed in section 3.3.

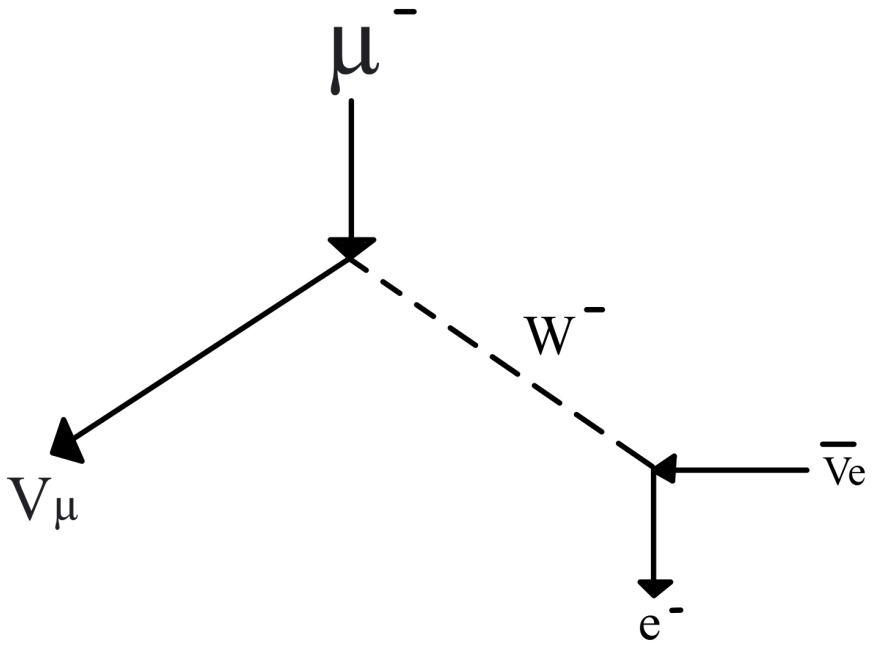

Figure 4: An illustration of the muon decay process. v_{mu} and $\overline{v}_e$ stand for the massless neutrinos. An electron is emitted during the muon decay process, which can excite the scintillator and generate light.

2 Experimental Procedure

2.1 Photomultiplier Tube & Amplifier

According to the photomultipliers manual (see reference [5]), a photomultiplier has four components: a photocathode, electron optics, a chain of dynodes, and an anode. As discussed in section 1.2, a pulse of light is generated as muons traverse or decay in the scintillator. These light pulses enter the PMT through the photocathode, a semi-transparent film. Due to the photoelectric effect, 20 % of electrons are converted from photon energy. Then, electron optics focus the electrons on the dynodes. There are 14 internal dynodes that amplify the electrons by a gain of 100 million. As a result, the anode collects the amplified electrons and outputs a negative voltage. An oscilloscope was used to test the output waveform by connecting the PMT output port to the oscilloscope's input channel, as shown in Fig 5.

Furthermore, the high voltage (HV) mode on the PMT was pre-set at 2300 volts. This voltage remained unchanged during the experiment because changing the HV level would cause noisy output for weeks.

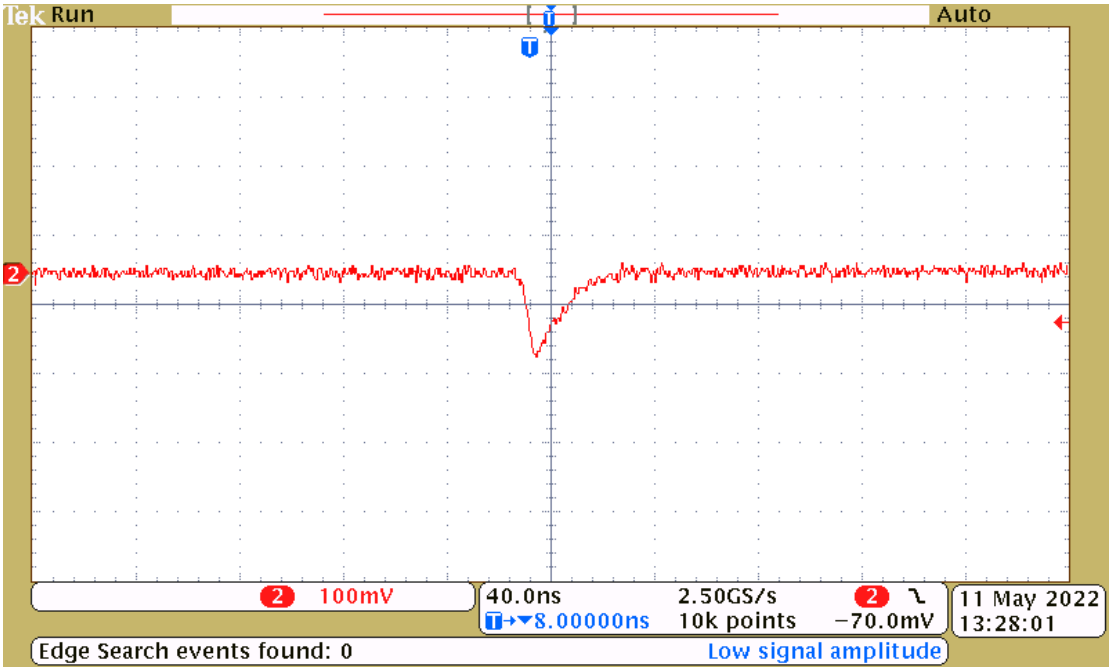

Figure 5: The scope screenshot of the output of PMT. It captures the pulse shape of the muon stop, which has a voltage per division setting of 100 mV / Div. As a result, the peak-peak value of the pulse is 150 mV with a min value of -150 mV.

As shown in Fig 3, when detecting the muon stop and decay pulses, the noises from the electronics, around 5 mV, could also be picked up. Therefore, an amplifier was connected to the PMT to widen the gap between the noises and muon decay pulse so that a threshold voltage level could be set to filter out the noises. The gain of the amplifier was calculated by the ratio of the p-p voltages in Fig 5 and 6. As a result, the amplifier had a gain of 4.

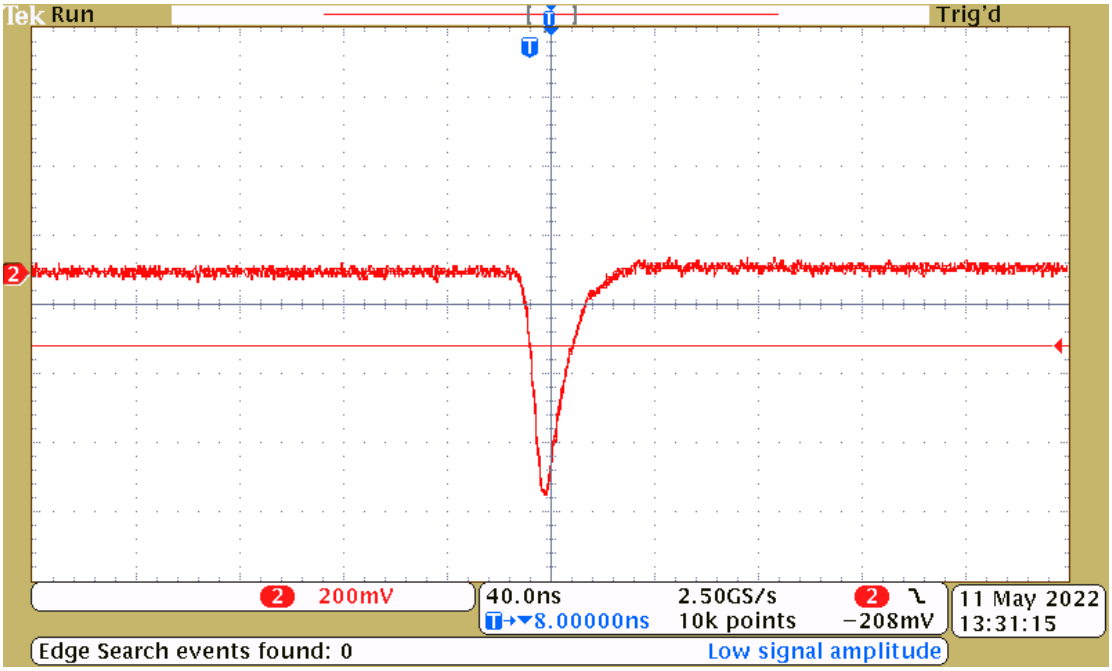

Figure 6: The scope screenshot of the output of PMT with an amplifier. It captures the pulse shape of the muon stop, which has a voltage per division setting of 200 mV

/ Div. As a result, the peak-peak value of the pulse is 600 mV with a min value of -600 mV. The gain of the amplifier = 600/150 = 4.

2.2 Discriminators

As shown in Fig 10, the discriminator was the first module connected to the PMT and its amplifier. It reads the output signal from PMT and outputs two identical signals separately to the delay gate and the coincidence module. The model of discriminator used in the experiment was LeCroy 623B, which has an adjustable threshold level from -30 mV to -1 V (see reference [4]). The function of the discriminator is to output a negative voltage around -800 mv when an input voltage reaches the threshold voltage level, as shown in Fig 7. The muon stop and decay pulse could not be detected if the threshold voltage was too high. Alternatively, if the threshold was too low, the undesirable noises from the electronics could also trigger the discriminator. As a result, a threshold of -70 mV was set by the screwdriver adjustment. -70 mV was chosen because it was far above the noise level and below the muon decay pulse's peak value.

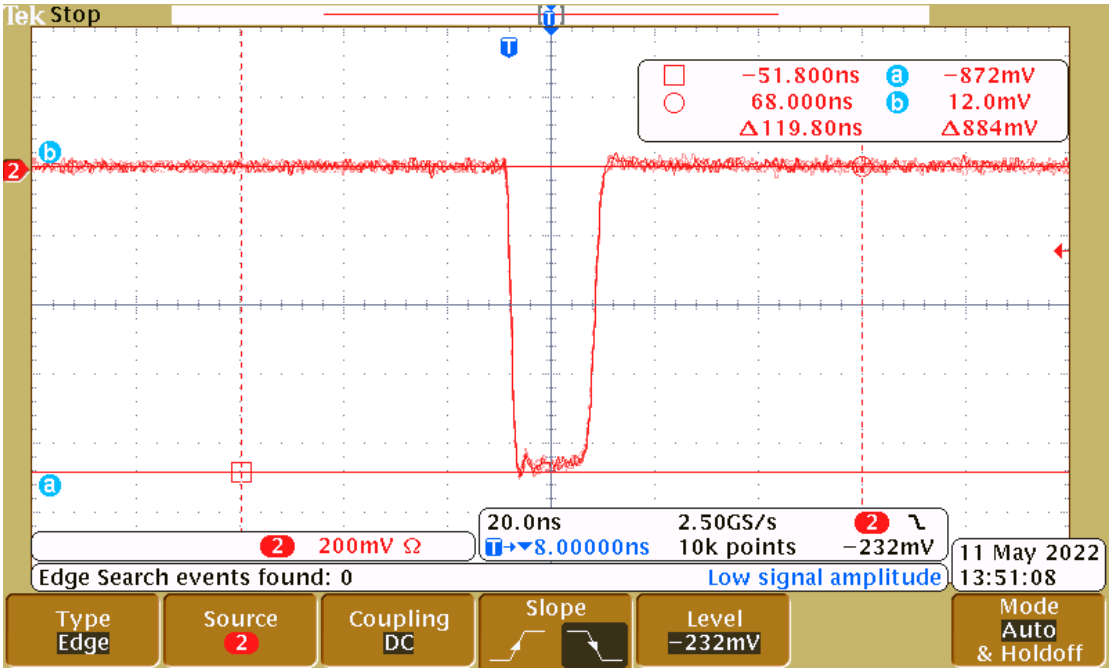

Figure 7: The scope screenshot of the output of the discriminator. It captures the pulse shape of the discriminator output when the input signal exceeds the threshold value. The voltage per division setting of 200 mV / Div. As a result, the peak-peak value of the pulse is 800 mV with a min value of -800 mV.

2.3 Dual Gate Generator

This experiment used a dual gate generator to create a 100 ns delayed pulse and a 10 μs gate. The model used for the dual gate generator was LRS 222. This module permits a gate duration from 100ns to 11 μs by the screwdriver adjustment (see reference [3]).

2.3.1 100 ns Delay Gate

The dual gate generator received the signal from one of the discriminator's outputs and created a 100 ns delayed pulse, as shown in Fig 8. This delayed signal was used to prevent the START and STOP signals from arriving at the TAC simultaneously, as noted in Fig 10. This 100ns delay guaranteed that the effect of the STOP signal was cleared before each timing sequence started. The resulting loss of counts of decay events in this 100 ns will be discussed in section 2.8.

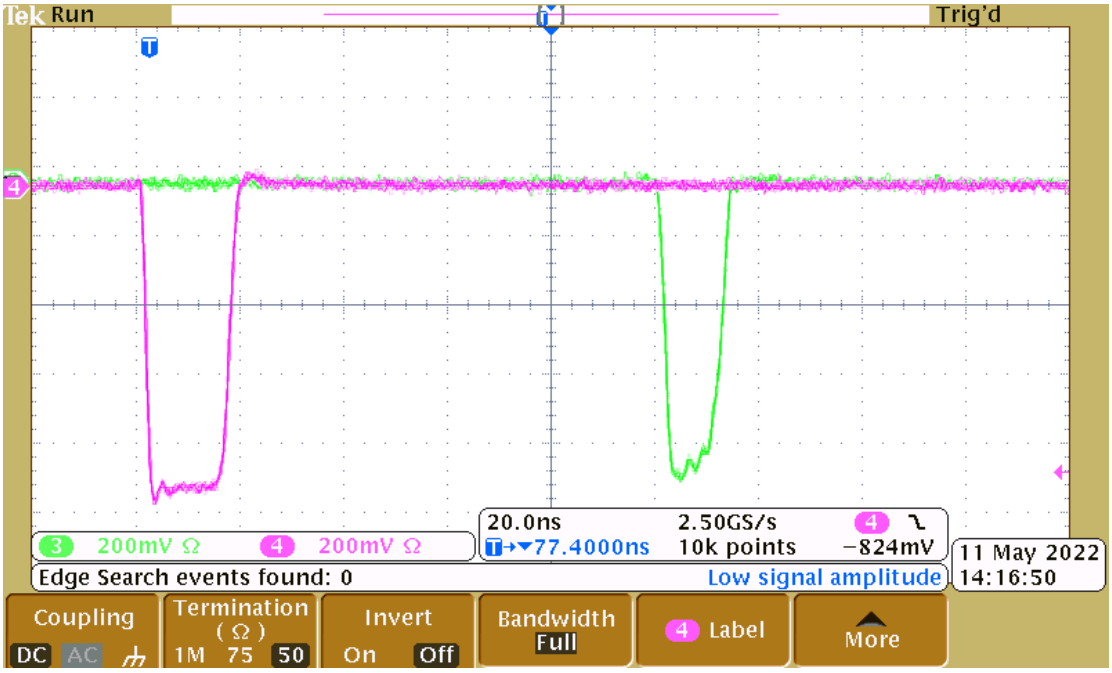

Figure 8: The scope screenshot of the input and output of the 100ns delay gate. Channel 4 represents the input pulse, and channel 3 represents the output pulse. The voltage per division setting for both channels is 200 mV / Div, and the time per division is 20.0 ns / Div. As a result, the peak-peak value of the pulse is 800 mV with a min value of -800 mV, and the time difference between two pulses is 100.0 ns.

2.3.2 10 μs Gate

Moreover, one of the discriminator's outputs went to the other input of the dual gate generator through the fan-out to create a 10 μs gate, as shown in Fig 9. This signal was subsequently output to the coincidence module to count the number of muon stop and decay events in a 10 μs interval.

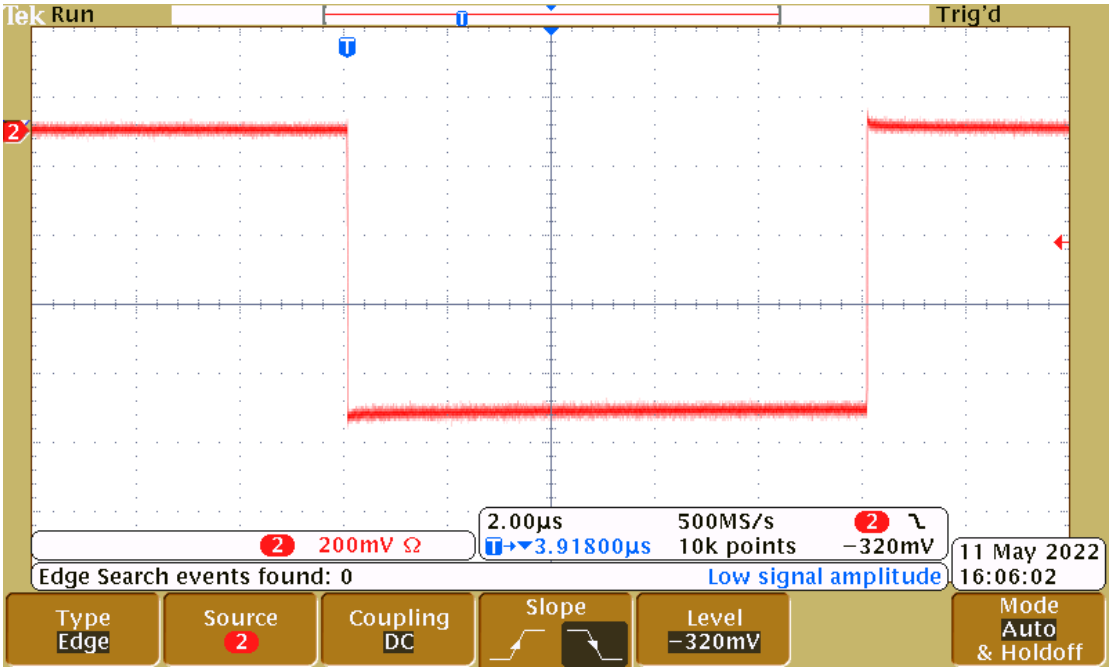

Figure 9: The scope screenshot of the output of the 10 μs gate. The voltage per division setting for both channels is 200 mV / Div, and the time per division is 2.00 μs / Div. As a result, the peak-peak value of the pulse is 800 mV with a min value of -800 mV, and the time duration between two pulses is 10 μs.

2.4 Fan-out Module

Tee connectors were not used in this circuit to spread the output signals because they have a mismatch impedance with the coaxial cables. This mismatch in impedance can cause pulse reflections in the logic circuit, resulting in signal interference. Nevertheless, the fan-out module, LRS 128L, could match the 50 Ohm impedance with the coaxial cables in the circuit (see reference [1]). Therefore, it was used as to duplicate the input signal and output them to the coincidence module, dual gate generator, and the TAC, as shown in Fig 10.

2.5 Coincidence Module & Dual Counter

The coincidence module, LRS 364, received the signal from the 10 μs gate from dual gate generator. Its coincidence level was set to 2 during the experiment to measure the counts of muon decay events. According to the LRS 364 manual (see reference [2]), the coincidence module would output a negative voltage to TAC as a STOP signal and to the counter B of the dual counter if two pulses are detected during the 10 μs interval.

Furthermore, the dual counter could display two numbers on counters A and B. Both counters incremented the display number by one when a negative input was detected. As shown in Fig 10, the input of counter A received the signal from the fan-out, meaning that its display number recorded the total number of muons detected. Counter B read the signal from the coincidence module, and its display number recorded the number of muons decayed.

2.6 Time to Amplitude Converter & Data Acquisition System

The Time to Amplitude Converter (TAC) received the input signal from the fan-out as START and the input signal from the coincidence module as STOP, as shown in Fig 10. The TAC generated a pulse with a linear rising voltage related to the time as it received the START signal. Consequently, the TAC output to the pulse to the pulse stretcher when the STOP signal arrived. An ideal TAC can generate a voltage that is linearly proportional to time. Therefore, a TAC calibration was conducted in the data analysis to check this linear relationship, discussed in section 3.2. Furthermore, the pulse stretcher shaped the pulse generated by the TAC into a pulse with uniform width and sent it to the Data Acquisition System.

Data Acquisition System (DAQ) was the primary source to record the data in an intelligible form. The DAQ recorded the ADC channel number where muon decay events occurred. The ADC channel number ranged from 0 to 4096, which corresponds to the 10μs interval of detecting muon decays.

2.7 Connections and Circuit Setup

Fig 10 illustrates the flow chart of the circuit. The coaxial cables used in the circuit connection had a resistance of 50 Ohms. Thus, there would not be signal reflection due to the impedance match. Moreover, the signal traveled at 2/3 c in the coaxial cable so that the length of the coaxial cable used was kept as short as possible to reduce the delay in signal transition. The actual circuit built is shown in Fig 11.

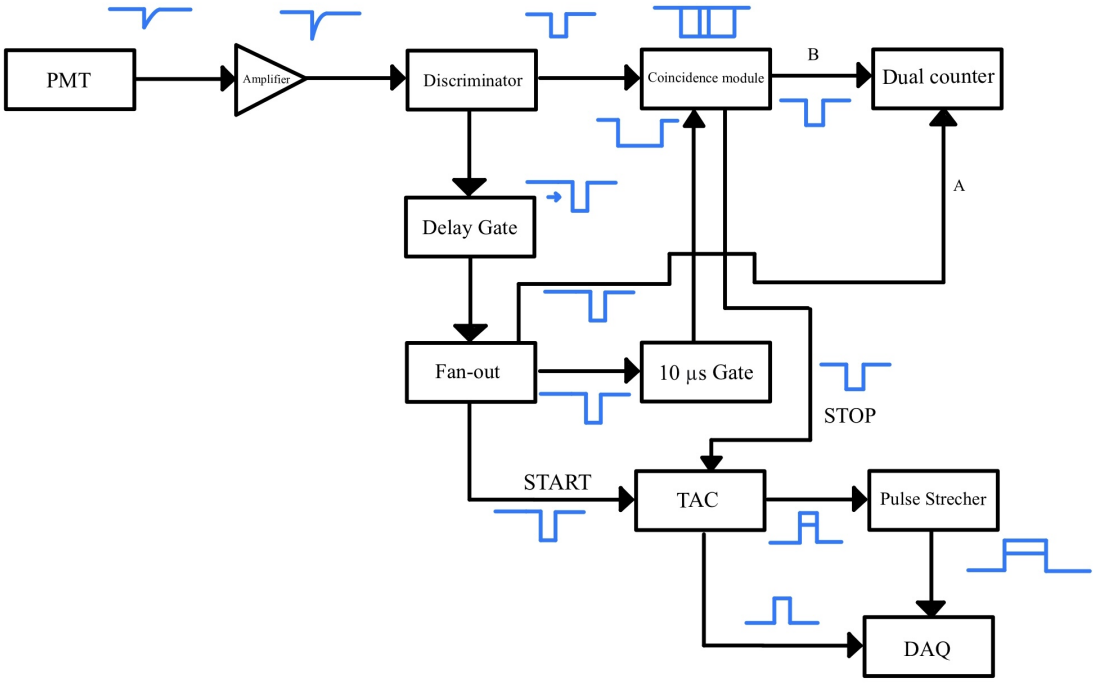

Figure 10: A detailed flow chart of the logic circuit. The pulse shape of the input and output signal are marked by blue. The start signal comes from PMT, and the discriminator will be triggered as muon stop and decay signals are detected. After a series of signal processing discussed in this experimental procedure, counter A of the dual counter records the total number of muons detected; counter B records the number of muons decayed during the experiment. Meanwhile, DAQ will only count the number of

muon decay events.

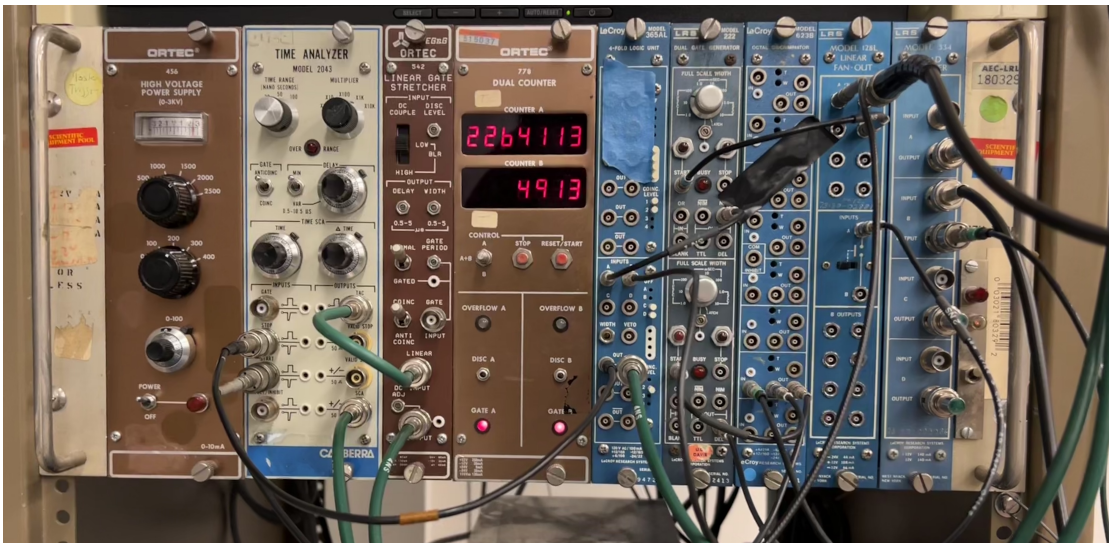

Figure 11: The picture of the actual circuit setup. All the coaxial cables used have a consistent resistance of 50 Ohms, preventing the signal reflection due to the impedance mismatch. Moreover, the length of the cables is kept as short as possible to reduce the transition delay. The number on counter A shows the total muons detected during a 120-hour run, and counter B shows the total muons decayed, which is around 0.2% of the total muons detected.

2.8 TAC Calibration

The TAC calibration was performed to check whether the TAC had a non-linear behavior in specific channels. In doing so, constant simulated muon stop and decay signals were injected into the input of the discriminator. Moreover, the discriminator and delay gate's outputs were connected to the STOP and START of the TAC module. The ADC channel numbers were recorded on DAQ while the time delay was controlled by the screwdriver adjustment on the front panel. The regions of interest are the points near ADC channels 0 and 4096. The calibration data resides in Muon data/TAC calibration on Google drive (see reference [10]). As shown in Fig 12, the TAC had a non-linear behavior in the ADC channel range [0, 130] and [4010, 4096].

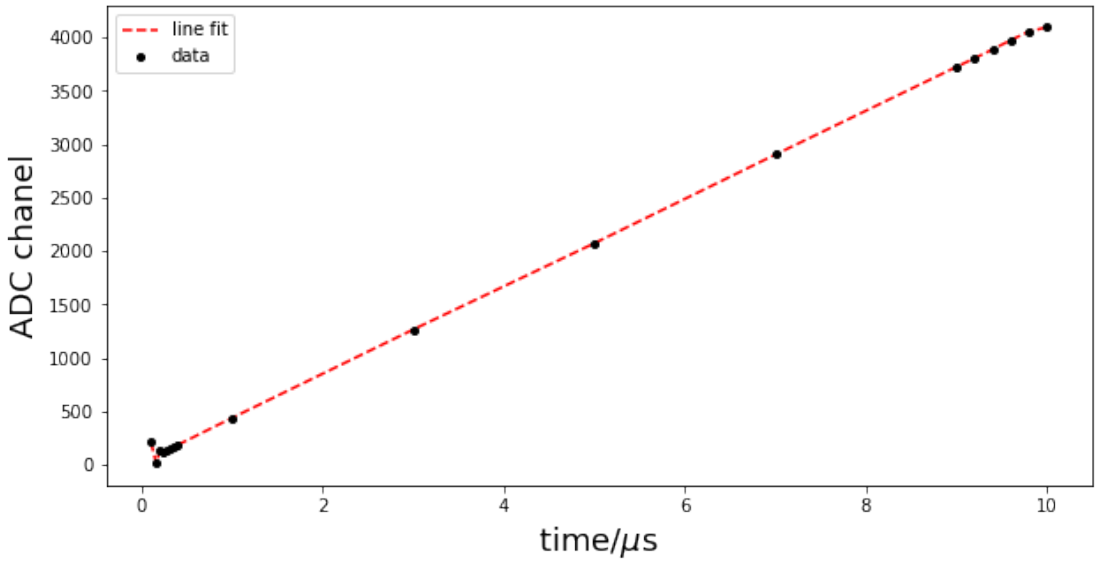

Figure 12: The plot of TAC calibration data. The data points used for calibration are marked in black. The region of interest is located at the beginning and the ending ADC channel. Therefore, each data point was incremented by 40 ns from 100ns to 400 ns. In the mid-range, each data point was incremented by 2 μs. Moreover, each data point was incremented by 200 ns from 9 μs to 10 μs. It is worth noting that the data in the range [100 ns, 200 ns] and [9.8 μs ,10 μs] exhibit non-linear behavior.

3 Data Analysis and Results

During the experiment, three runs were performed, including a 120-hour run (4 hours to 5 days), a 44-hour run (4 hours to 2 days), and a 120-hour run (4 hours to 5 days) with 20 μs time intervals. The counts of muon decay events and their ADC channel number were recorded in the data acquisition system. Furthermore, the expected muon decay function was given by Melissinos in his book "Experiments in Modern Physics," as shown in Eqn 8. N(t) indicates the number of decayed muons at a given time, N_0 represents a constant number, B denotes the background counts during the experiment, and τ defines the muon mean lifetime.

$$N(t) = N_0 \cdot e^{-\frac{t}{\tau}} + B \tag{8}$$

The dataset containing the counts of muon decay events and ADC channel number resides in Muon data/Muon decay on Google drive (see reference [10]).

3.1 Data Binning and Line Fit

Fig 13 illustrates the raw distribution of muon decay events in a 120-hour run . As a result, 4518 decay events were recorded during the experiment. The muon decay rate was approximately 0.01 per second, close to the prediction made in section 1.2. However, it is worth noting that there is a significant peak around ADC channel 0 and a small peak around ADC channel 4000. These abnormal peaks were caused by the TAC non-linear behavior measured in section 2.8.

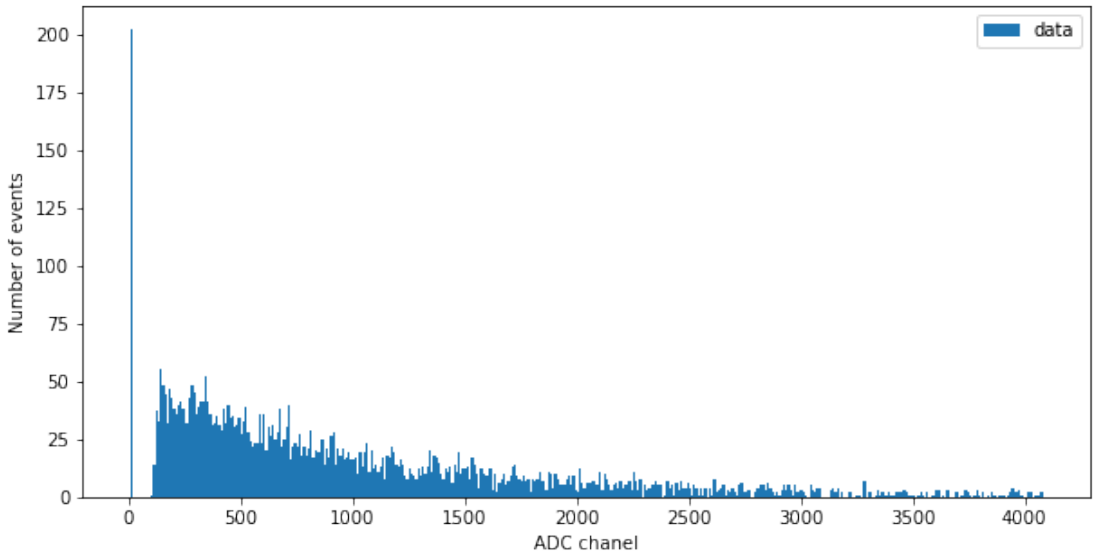

Figure 13: The distribution of unbinned data in a 120-hour run. The vertical axis represents the decay counts in each channel, and the horizontal axis indicates the ADC channel number. An abnormal spike at the left and right of the data distribution agrees with the TAC non-linear behaving region. Therefore, channels [0, 130] and [130, 4010] are edited out in the data analysis.

Furthermore, the data is refined to 60 bins for 44-hour run and 120-hour run to perform an exponential line fit described in Eqn 8, and the error bar of each bin is calculated by taking the square root of the counts in the bin. Fig 14 and 15 shows the distribution of muon decay events in a 44-hour run and a 120-hour run while the data points in ADC channel range [0,130] and [4010,4096] are edited out. In addition, the data from the two runs are jointly analyzed, as shown in Fig 16. The number of points, related reduced χ^2, and function parameters are included in Table 1.

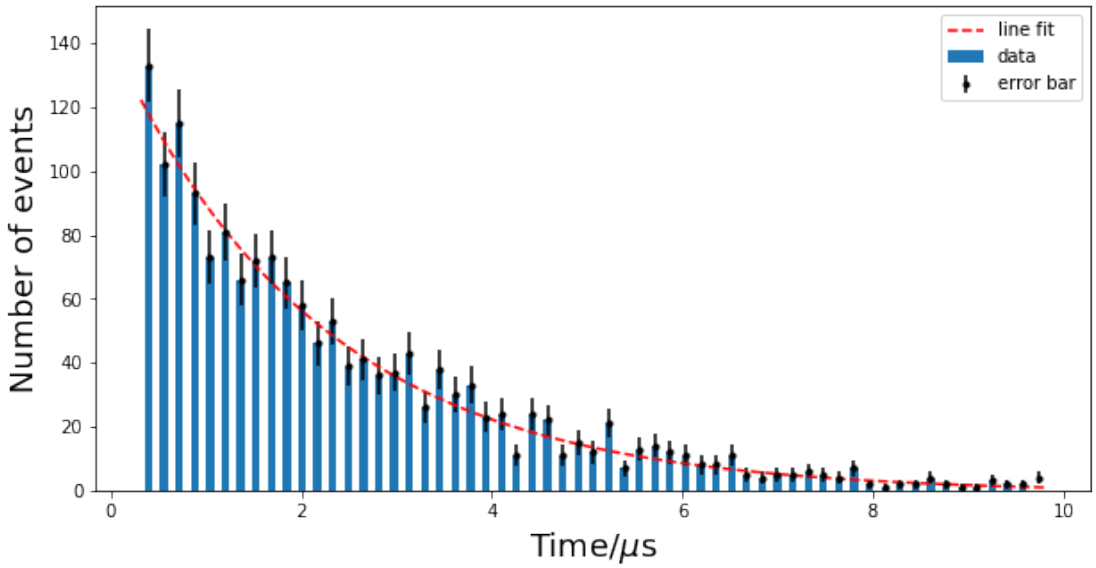

Figure 14: The distribution of data in 60 bins in a 44-hour run. The vertical axis represents the decay counts in each bin, and the horizontal axis indicates the time interval

converted from the ADC channel number. The abnormal spike at the left and right of the data distribution is removed in the analysis. Error bars are calculated by taking the square root of decay counts in each bin, marked in black. An exponential line fit is applied to this data distribution, marked by the red dashed line.

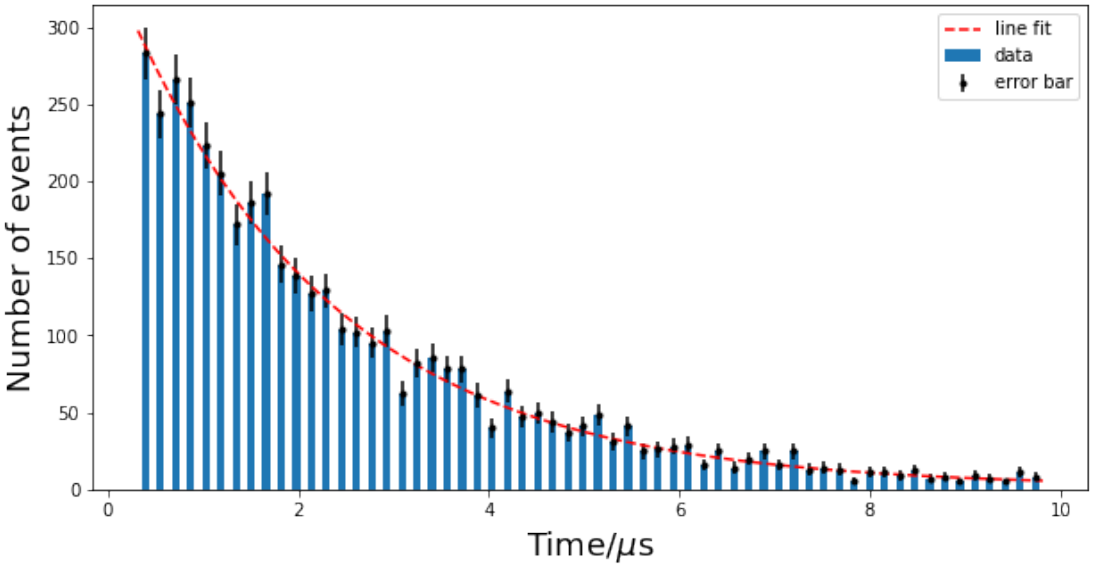

Figure 15: The distribution of data in 60 bins in a 120-hour run. The vertical axis represents the decay counts in each bin, and the horizontal axis indicates the time interval. Error bars are calculated by taking the square root of decay counts in each bin, marked in black. The abnormal spike at the left and right of the data distribution is removed in the analysis. An exponential line fit is also applied to this data distribution, marked by the red dashed line.

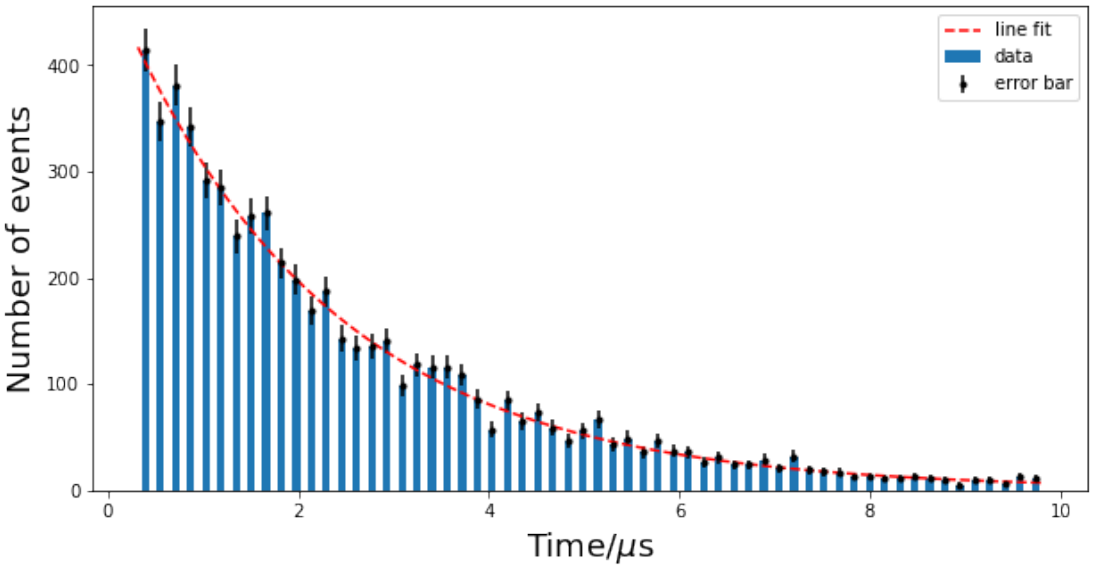

Figure 16: The combination of distribution of data in 60 bins in a 44-hour run a 120-hour run. The vertical axis represents the decay counts in each bin, and the horizontal axis indicates the time interval. Error bars are calculated by taking the square root of decay

counts in each bin, marked in black. The abnormal spike at the left and right of the data distribution is removed in the analysis. An exponential line fit is also applied to this data distribution, marked by the red dashed line.

Number of points	N_0	τ/μ s	Background counts	Reduced χ^2
1785	142 ± 6	2.19 ± 0.10	-0.7 ± 0.7	0.99
4518	342 ± 10	2.22 ± 0.07	1.6 ± 1.2	1.13
6303	479 ± 11	2.23 ± 0.06	1.2 ± 1.4	1.20

Table 1: The τ_μ ranges from 2.19 to 2.23 in three distributions. All the exponential line fits have reduced χ^2 close to 1, indicating that the exponential function is well-fitted to the data. However, the background counts have significant uncertainties.

Although the average muon lifetime remains consistent and the line fit has a reduced χ^2 close to 1, the fitted parameters for background count have low precision and even negative values. The background counts come from the two muon stop events instead of a muon stop event followed by a muon decay event. As shown in Fig 17, two muons pass through the medium with 10 μs or the second muon pass through the medium before the first muon decays. Therefore, the coincidence detects two pulses in the 10 μs window and miscounts this accidental event as a muon decay. The negative background counts do not make physical sense because muons cannot be counted "negative times" in this process. Thus, another 120-hour run with muon decays' detection interval extending from 10 μs the 20 μs was performed to increase the background precision.

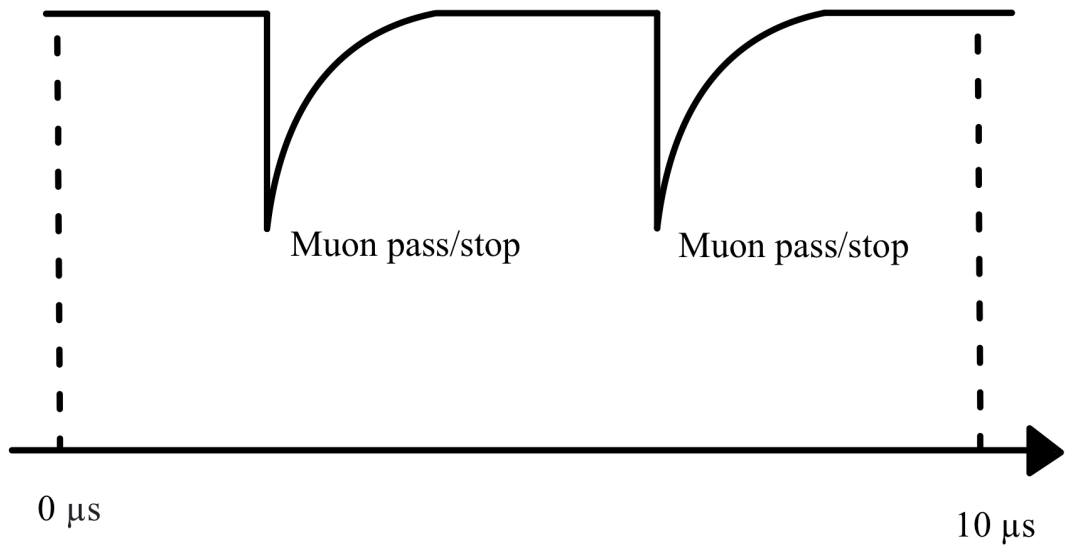

Figure 17: An illustration of the occurrence of background counts during the 10 μs interval. During the 120-hour run, two muons may pass through the scintillator during the 10 μs interval. Both pulses can trigger the discriminator. As a result, the coincidence module will miscount this event as a "decay." The Poisson distribution can be applied to determine the probability of this event.

3.2 Background Counts Precision

The detection of muons follows a Poisson distribution, as described in Eqn 9. P represents the probability of two muons arriving within 20 μs, λ denotes the mean rate of incoming muon per 20 μs, and n stands for the number of successes.

$$P = \frac{\lambda^n e^{-\lambda}}{n!} \tag{9}$$

As a result, the expected probability and background counts per bin can be derived from Eqn 10 and 11, where 1.08×10^{-4} is the average muon incoming rate per 20 μs and 2.088×10^{-10} is the number of 20 μ intervals in 120 hours.

$$P = \frac{(1.08 \times 10^{-4})^2 \cdot e^{-1.08 \times 10^{-4}}}{2!} \approx 5.8 \times 10^{-9} \tag{10}$$

$$Background\,counts\,per\,bin\,(in\,20\mu s) = \frac{5.8 \times 10^{-9} \times 2.088 \times 10^{10}}{60} = 2.0 \tag{11}$$

Fig 18 shows the distribution of muon decay events in a 120-hour run with 20 μs detecting window. Furthermore, the number of points, related reduced χ^2, and function parameters for both 120-hour runs with 10 μs and 20 μs intervals are included in Table 2 for comparison. It is worth noting that the data points collected are reduced in a 120-hour run with 20 μs interval because one detection cycle must wait for 20 μs for muons that passed through the scintillator and did not decay. As a result, more time was wasted in this waiting process.

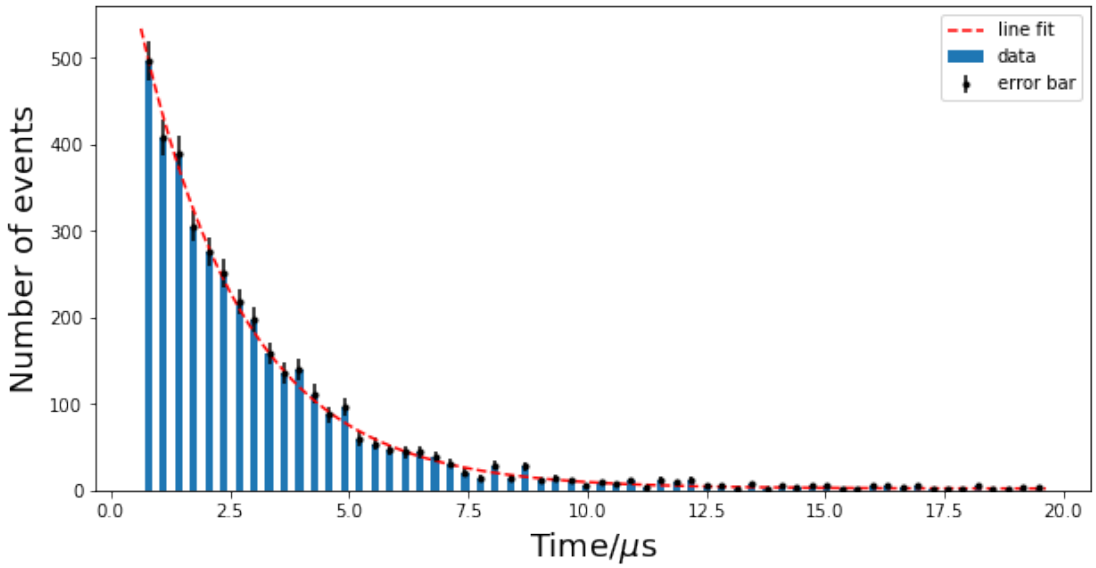

Figure 18: The distribution of data in 60 bins in a 120-hour run with 20 μs interval. The vertical axis represents the decay counts in each bin, and the horizontal axis indicates the time interval. An exponential line fit is also applied to this data distribution to improve the precision of the background counts, marked by the red dashed line. Error bars are calculated by taking the square root of decay counts in each bin, marked in black.

Number of points	N_0	τ/μ s	Background counts	Reduced χ^2
4518	342 ± 10	2.22 ± 0.07	1.6 ± 1.2	1.13
4449	709 ± 20	2.20 ± 0.04	2.2 ± 0.4	1.19

Table 2: The τ_μ ranges from consistent in two distributions. Both the exponential line fits have reduced chi^2 close to 1, indicating that the exponential function is well-fitted to the data. The background count in 20 μs has a much smaller uncertainty compared to the background counts in 10 μs. It is also worth noting that the precision for τ_μ is also improved.

The background count precision for the 20 μs interval increases a lot compared to the 10 μs interval. Background counts of 2.2 ± 0.4 also agrees with the calculation in Eqn 11. Furthermore, a similar calculation for background counts in the 20μs range can also be applied to the background counts in the 10μ range, as shown in Eqn 12. The result falls within the 1.1 ± 0.2 range, derived from the dividing the background counts for 20 μs by 2.

$$Background\,counts\,per\,bin\,(in\,10\mu s) = \frac{2.9 \times 10^{-9} \times 4.176 \times 10^{10}}{100} = 1.2 \tag{12}$$

As a result, the exponential line fit model with statistical uncertainty is:

$$N(t) = (479 \pm 11) \cdot e^{-\frac{t}{(2.23 \pm 0.06)\mu s}} + (1.1 \pm 0.2) \tag{13}$$

3.3 μ^- Capture

As mentioned in section 1.2, two types of muons: μ^- and μ^+, were detected during the experiment. However, μ^- can be attracted to the carbon nucleus during the decay process, and the Bohr radius of μ^- orbiting the carbon nucleus can be calculated from Eqn 14.

$$R_{Bohr} = \frac{\hbar}{m_\mu \cdot c \cdot \alpha \cdot Z} \tag{14}$$

$\hbar$ represents the reduced plank constant, m_μ denotes the mass of the muon, c stands for the speed of light, α indicates the fine-structure constant, and Z represents the proton number in a carbon atom. As a result, the Bohr radius of a μ^- is smaller than the radius of the carbon nucleus. In other words, μ^- can be captured by the carbon nucleus during the decay process, as shown in Fig 19.

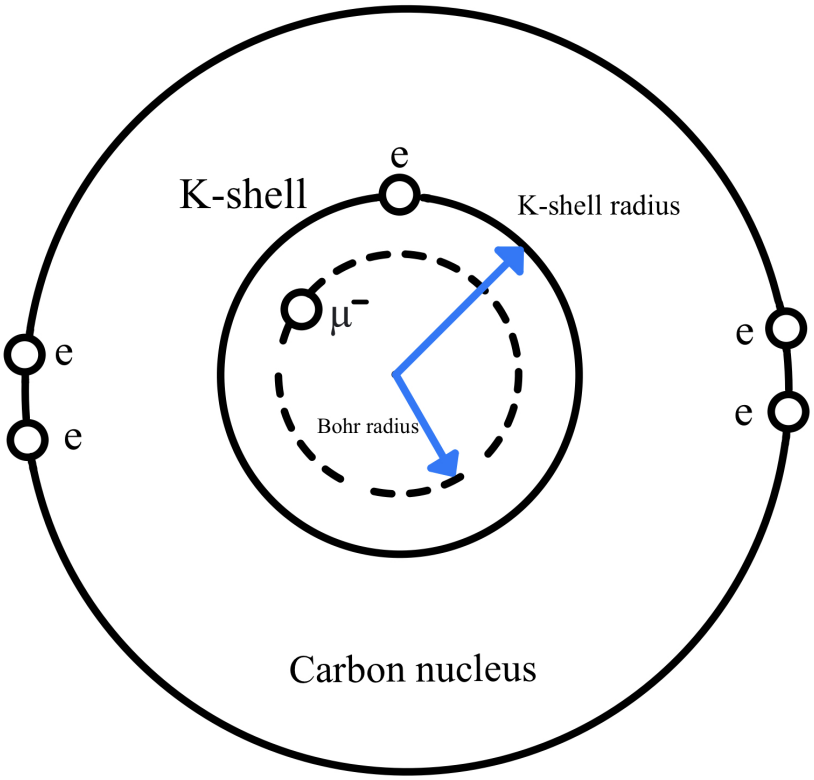

Figure 19: An illustration of the structure of a carbon nucleus when a μ^- is captured. The inner circle represents the K-shell of the carbon nucleus. As μ^- traverses the medium, it can be attracted to a carbon nucleus and orbit around it. As a result, the Bohr radius of the μ^-, marked by the black dashed line, is smaller than the radius of the carbon K-shell radius, indicating a μ^- is captured by the carbon nucleus.

The capture process and the K-capture time are described in Eqn 15, given by Evans in his book "The Atomic Nucleus" in 1955.

$$\begin{aligned} \mu^- + \mathrm{p} &\longrightarrow \mathrm{n} + \mathrm{v} \\ \tau_c &\approx 10^{-7} \times (\frac{82}{Z})^4 \end{aligned} \tag{15}$$

Nevertheless, the scintillator used in the experiment cannot distinguish between μ^- and μ^+. Therefore, the τ_μ measured in the experiment was the combination of τ_{μ^-} and τ_{μ^+}, which can be represented as τ_{eff}. Eqn 16 is applied to correct for the τ_μ.

$$\frac{1}{\tau_{eff}} = \frac{1}{\tau_\mu} + \frac{1}{\tau_c} \tag{16}$$

The τ_{eff} measured is 2.23 μs and τ_c captured by carbon equals $10^{-7} \times (\frac{82}{6})^4 = 3.48\, ms$. Thus, τ_μ can be derived from Eqn 17.

$$\tau_\mu = \frac{\tau_{eff} \times \tau_c}{\tau_c - \tau_{eff}} \tag{17}$$

Furthermore, an approximation of τ_μ is made based on Melissinos's calculation that the correction for the ratio of μ^- to μ^+ in the cosmic ray is 4%, as indicated in Eqn 18.

$$\tau_\mu = \tau_{eff} \times (100\% + 4\%) \tag{18}$$

Therefore, the corrected muon mean lifetime is:

$$\tau_\mu = (2.23 \pm 0.06)\,\mu s \times 1.04 = 2.319 \pm 0.062\,\mu s(stat) \tag{19}$$

3.4 Sources of Systematic Errors

The primary source of systematic errors came from the TAC calibration. Although the non-linear region of the TAC was edited out in the analysis, the cutoff point of the linear region chosen was not definitive. From Fig 12, the linear region of TAC started around ADC channel 100 up to 150 and ended around 4000 up to 4050. Furthermore, the methodology could also cause a systematic error because 250 data points were disregarded. The shape of the distribution in the range of beginning and ending channels might have an impact on the τ_μ. However, the shape of the distribution cannot be restored from edited-out data. The systematic error estimation comes from adjusting the range of ADC channels from [100, 4050] to [150, 4000] and observing the change in τ_μ, as shown in Table 3.

ADC channel range	τ/μ s	Reduced χ^2
100 - 4050	2.37 ± 0.07	1.79
110 - 4040	2.28 ± 0.06	1.31
120 - 4030	2.23 ± 0.06	1.35
130 - 4020	2.23 ± 0.06	1.29
140 - 4010	2.23 ± 0.06	1.45
150 - 4000	2.25 ± 0.06	1.17

Table 3: The τ_μ is dependent on the chosen range of the ADC channel. τ_μ ranges from 2.23 to 2.28 as the range of the ADC channel varies. The τ_μ in the first row is not trustworthy because it has the largest reduced χ^2 and the most significant uncertainty.

The τ_μ from the ADC channel range from 100 to 4050 has the largest reduced χ^2 squared and statistical error. However, the rest of τ_{mu} varies from 2.23 μs away from 2.28 μs and has reduced χ^2 close to 1. Hence, the estimation of systematic error is ± 0.03. By applying the 4% capture effect correction, the muon lifetime is:

$$\tau_\mu = (2.23 \pm 0.06 \pm 0.02)\,\mu s \times 1.04 = 2.319\,\mu s \pm 0.062\,\mu s(stat) \pm 0.031\,\mu s(syst) \tag{20}$$

4 Discussion

The measured muon lifetime is 5% smaller than the expected value, 2.196 μs, which falls within an acceptable range. As discussed in section 3.3, a 4% of capture effect correction is applied to the measured τ_μ. However, this capture interaction is complicated, indicating that the 4% correction coefficient is not necessarily an accurate approximation. A more accurate measured tau_μ can be obtained by separating the μ^+ and μ^- particles by accelerators. Therefore, the μ^+ and μ^- lifetime can be derived independently. The approximation for the ratio of μ^- to μ^+ in the cosmic ray is no longer needed. However,

many other factors can have an impact on the measured τ_μ value in the experiment and analysis, discussed in the following subsections.

4.1 Reduced χ^2 and τ_μ vs. Number of Bins

In the analysis, the original data was re-binned into 60 bins to conduct an exponential line fit, which generated the τ_μ as the parameter in the function. However, different numbers of bins can result in different exponential line fits and reduced χ^2 values, as shown in Fig 20. The reduced χ^2 remains constant around one as the number of bins is above 60, suggesting that the exponential function is well-fitted. However, as shown in Fig 21, the τ_μ can vary from 2.21 μs to 2.26 μs as the number of bins ranges from 60 to 150. As a result, the measured τ_μ is dependent on the number of bins. This correlation indicates that the data analysis has an unobserved bias, which can shift the τ_μ values.

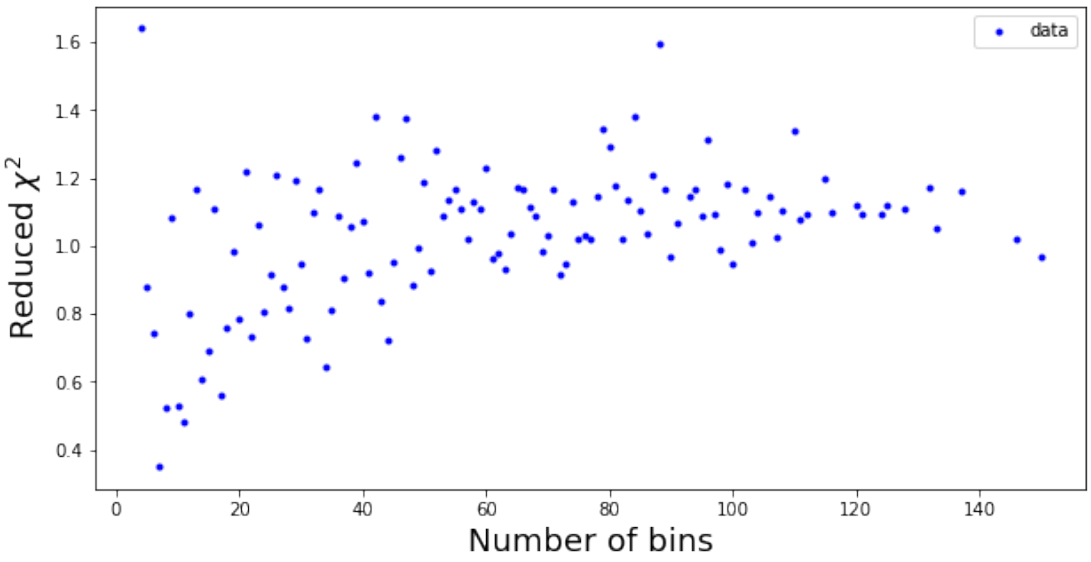

Figure 20: The plot demonstrating the relationship between reduced χ^2 and the number of bins in a 120-hour run. The reduced χ^2 remains constant around 1 as the number of bins increases. However, the number of bins below 30 bins produces reduced χ^2 ranging from 0.4 to 0.8. It implies that a bias in analysis can occur if too many data points are categorized in a wide bin.

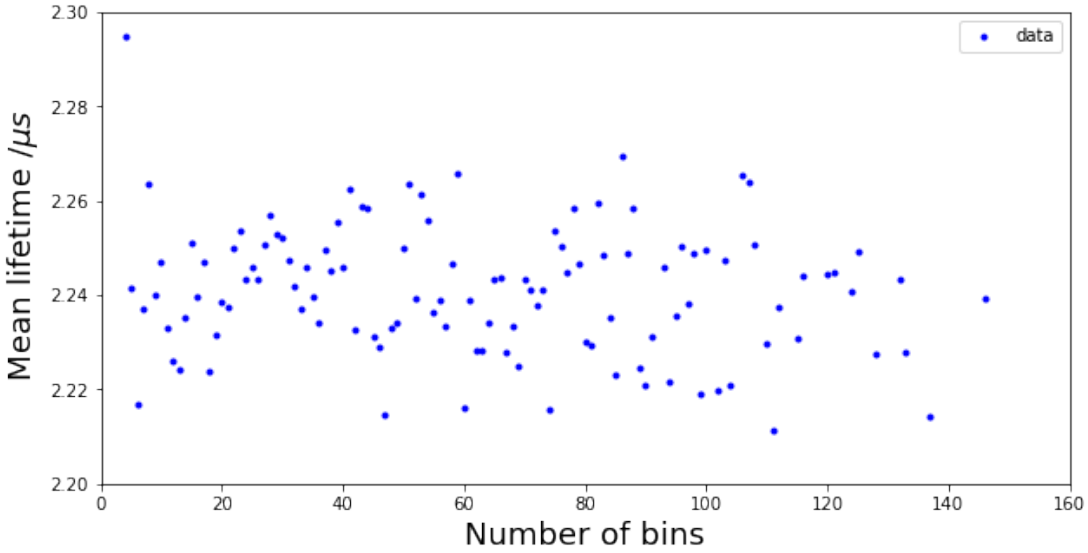

Figure 21: The plot demonstrating the relationship between τ_{mu} and the number of bins in a 120-hour run. The reduced τ_{mu} ranges from 2.26 to 2.21 even with reduced χ^2 close to 1, indicating the τ_{mu} is dependent on the number of bins.

4.2 Number of Decays Mismatch

There is a discrepancy of 10 % between the number of data recorded in the DAQ and the number displayed in counter B. In other words, the DAQ ignored 10 % of decay events during the experiment. It remains questionable whether this loss of data was a random process. One potential possibility is that the data points that DAQ disregarded were located at a particular data channel range, causing an unobserved measurement bias in the data recording. As a result, the calculated τ_μ becomes inaccurate.

4.3 Different Time Windows for Muon Detection

As discussed in section 3.2, two runs with 10 μs and 20μs intervals were performed to improve the background precision. Nevertheless, the τ_μ value in the 20μs interval has also changed from 2.2 μs to 2.0 μs with a smaller uncertainty. It implies that τ_μ is dependent on different time windows for muon detection. From the current data, it seems that the τ_μ is more precise and closer to 2.196 μs as time windows for muon detection increase. If more time was available, multiple runs with different detecting intervals could be performed to investigate the relationship between the τ_μ and detecting intervals.

5 Conclusion

This experiment aims to measure the mean lifetime of muons originating from the high-energy collision between the atmosphere and the cosmic ray. The measurement result of muon lifetime, τ_{mu}, is 2.319 μs $\pm$ 0.062 μs (stat) $\pm$ 0.031 μs (syst), which is about 5% different from the published value, 2.196 μs. Further TAC calibration and separation of μ^+ and μ^- can be conducted to improve the accuracy and precision of the muon lifetime. In this experiment, a plastic scintillator connected with an amplified photomultiplier tube was used to detect muons. Moreover, a logic circuit including a

discriminator, dual gate generator, coincidence module, and TAC was used to measure the muon lifetime. In the data analysis part, it is found out thatτ_{mu} can be affected by several factors such as the number of bins and duration of detecting interval.

6 Acknowledgments

Acknowledging the help of lab partner, Garrett Wilson, who had been helpful and showed great teamwork during the experiment.

References

[1] Electronic Systems Engineering 128L Dual lin oct fan-out manual form Fermi Laboratory

[2] Equipment Logistics Services 364/364N Dual 4-Fold Logic manual form Fermi Laboratory

[3] NIM Model 222/222N Dual Gate Generator" manual.

[4] NIM Model 623B Octal Updating Discriminator" manual.

[5] Photomultipliers". In: Encyclopedia of Biomedical Engineering, Silvano Donati, University of Pavia Pavia, Italy.

[6] PHY 122B Lab manual "Determination of the Muon Lifetime".

[7] Melissinos, Adrian C., and Jim Napolitano. Experiments in Modern Physics. Academic Press, 2011, pp. 406–9.

[8] Model 2145 Time-to-Amplitude Converter/SCA manual

[9] Robley Duarglison Evans. The Atomic Nucleus. Mcgraw-Hill, 1955, pp. 42–43.

[10] Measurement data is available on https://drive.google.com/drive/folders/1VIBr7udRY9gbP4Wjv7qfADAi60jLjRfp?usp=sharing.